American Mineralogist, Volume 91, pages 1170–1177, 2006

The crystal structure of piergorite-(Ce), $Ca_8Ce_2(Al_{0.5}Fe^{3+}_{0.5})_{\Sigma1}(\square,Li,Be)_2Si_6B_8O_{36}(OH,F)_2$: A new borosilicate from Vetralla, Italy, with a modified hellandite-type chain

MASSIMO BOIOCCHI,[1,2,*] ATHOS CALLEGARI,[2,3] AND LUISA OTTOLINI[3]

[1]Centro Grandi Strumenti, Università degli Studi di Pavia, via Bassi 21, I-27100 Pavia, Italy
[2]Dipartimento di Scienze della Terra, Università degli Studi di Pavia, via Ferrata 1, I-27100 Pavia, Italy
[3]CNR—Istituto di Geoscienze e Georisorse (IGG), Sede di Pavia, via Ferrata 1, I-27100 Pavia, Italy

ABSTRACT

Piergorite-(Ce) is a new mineral found at Tre Croci, Vetralla, Italy with simplified formula $Ca_8Ce_2(Al_{0.5}Fe^{3+}_{0.5})_{\Sigma1}(\square,Li,Be)_2Si_6B_8O_{36}(OH,F)_2$. It occurs as strong intergrowths of small crystals, colorless to pale yellow, associated with sanidine, mica, magnetite, rutile, titanite, and other Th-U-REE bearing minerals, in miarolitic cavities of a syenitic ejectum. Piergorite-(Ce) is biaxial negative, $n_\alpha = 1.717$ (1), $n_\beta = 1.728$ (1), and $n_\gamma = 1.735$ (1), $2V_{meas} = 68(2)°$, $X = \mathbf{b}$, and $Z \wedge \mathbf{c} = 7(1)°$. Crystals show tabular habit and a very good {010} cleavage; twinning along the $(30\bar{1})$ plane produces "L" forms. The three strongest lines in the simulated powder diffraction pattern (d_{obs}, I, hkl) are: 2.65 Å, 100.0, (213, $\bar{4}$13); 1.91 Å, 48.3, (223, $\bar{4}$23, 821); 2.90 Å, 44.9, ($\bar{6}$03, $\bar{6}$12). The structure was solved by Patterson synthesis from X-ray diffraction data [monoclinic, space group $P2/a$, $a = 28.097(3)$ Å, $b = 4.777(1)$ Å, $c = 10.236(2)$ Å, $\beta = 96.81(1)°$, $V = 1364.2(7)$ Å^3, Z = 2] and was refined to a final $R_{obs} = 0.059$ for 6480 Fo with $I_o > 3\sigma(I_o)$. The structure shows similarities with the hellandite group because Si and B tetrahedra form chains along **c**. Hellandite structure is characterized by a single chain of five-membered rings, whereas piergorite-(Ce) shows a double chain of five-membered rings interconnected by a single octahedral site to form a three-dimensional framework containing five independent eightfold-coordinated M sites and a partly occupied T-cavity.

Keywords: New mineral, piergorite-(Ce), borosilicate, crystal structure, SIMS, hellandite

INTRODUCTION

During the last few years, the crystal-chemical knowledge of REE-minerals has been improved by the study of samples from the Vico volcanic complex (Viterbo province, Italy). In particular, among the accessory phases of the syenitic ejecta named "sanidiniti," two new mineral species were found: vicanite-(Ce) (Ballirano et al. 2002) and peprossiite-(Ce) (Callegari et al. 2000). Both minerals show peculiar structural features: the $Si_3B_3O_{18}$ polyanion in vicanite-(Ce), and the square pyramidal coordination for Al in peprossiite-(Ce). Furthermore, REE-rich hellandites from these ejecta were studied to clarify the crystal-chemical properties of hellandite-type minerals (Oberti et al. 2002), and other interesting or rare mineral species were found and characterized [e.g., stillwellite-(Ce) (Callegari et al. 1992), baddeleyite (Della Ventura et al. 1986)].

New samples from the Vico complex contain platy, colorless to pale yellow crystals, very similar to the associated and well-formed hellandite crystals but significantly smaller in size. A preliminary analysis showed that the unit-cell parameters were different from those of hellandite and a complete crystal chemical study was carried out, combining a single-crystal X-ray diffraction study together with electron and ion microprobe analyses. The identified crystals resulted in a new mineral species and the complete description is reported here.

The mineral has been named piergorite-(Ce), an acronym from the name of two Italian collectors that have provided us with the sample in study: Giancarlo Pierini and Pietro Gorini. Both are well known, appreciated, and keen collectors of minerals, and are always available to provide the scientific community with specimens for mineralogical research. The new mineral and its name were approved by the Commission on New Minerals and Mineral Names (CNMMN) (I.M.A. 2005-008). The approved mineral name has been corrected by means of a Levinson modifier during the preparation of this manuscript, following the suggestion of one of the reviewers and in agreement with the chairman of the CNMMN. Type material (the analyzed crystal and crystal concentrate from the same rock sample) has been deposited at the Museo di Mineralogia, Dipartimento di Scienze della Terra, Università degli Studi di Pavia, Italy with catalog number 2005-001 OL.

OCCURRENCE

Piergorite-(Ce) crystals have been found in myarolitic cavities inside a volcanic ejectum of syenitic composition from the Vico complex (Tre Croci locality, Vetralla, Viterbo province, Italy). The host rock consists mainly of K-feldspar (sanidine) and minor plagioclase, clinopyroxene, and magnetite. Other accessory minerals are hellandite-(Ce), titanite, nosean, baddeleyite, afghanite, danburite, biotite, rutile, thorite, vonsenite, and homilite. The mineral probably formed as a late-stage crystallization product occurring on the surface of the K-feldspar matrix as isolated crystals or submillimetric wisps.

* E-mail: boiocchi@crystal.unipv.it

PHYSICAL AND OPTICAL PROPERTIES

Piergorite-(Ce) occurs as platy or acicular crystals, colorless to pale yellow, with a maximum dimension of 300–400 μm (Fig. 1). Crystals have perfect {010} cleavage and are characterized by polysynthetic twinning on {100}; frequently, they show L-shaped form by further twinning on the {30$\bar{1}$} (Fig. 2). Neither the hardness nor the density could be measured because of the brittle character and the small size of the crystals. The calculated density is 3.67 g/cm^3, while the hardness should be similar to that of hellandite (5½– 6 on the Mohs scale) since several crystal-chemical features of piergorite-(Ce) strongly resemble those of hellandite-group minerals.

Piergorite-(Ce) is biaxial negative, $n_\alpha = 1.717$ (1), $n_\beta = 1.728$ (1) and $n_\gamma = 1.735$ (1) (for $\lambda = 589$ nm); $2V_{meas} = 68(2)°$, and $2V_{calc} = 77(10)°$. Optical orientation is: $X = \mathbf{b}$ and $Z \wedge \mathbf{c} = 7(1)°$. Crystals are translucent, vitreous, without dispersion effects or pleochroism. A Gladstone-Dale calculation gives a compatibility index of 0.012, which is regarded as excellent (Mandarino 1981).

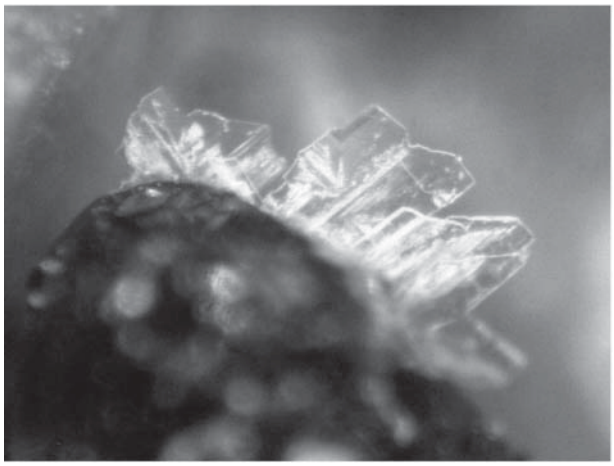

FIGURE 1. Group of platy-elongated crystals of piergorite-(Ce) from Vetralla (Italy). The maximum length of crystals is 400 μm.

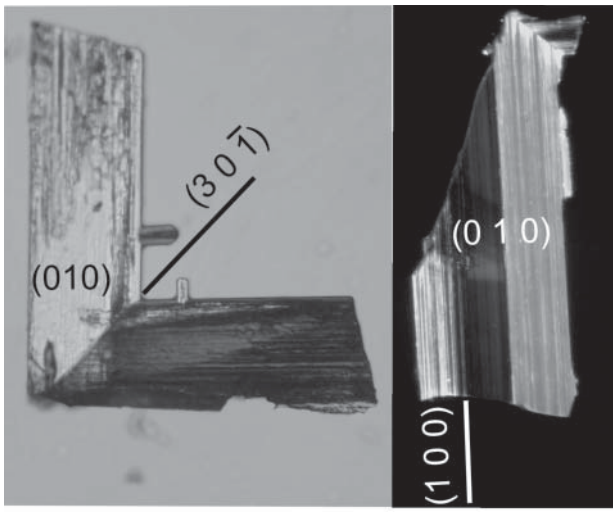

FIGURE 2. Piergorite-(Ce) in transmitted polarized light shows two kinds of twinning: along (30$\bar{1}$) (left) and (100) (right). In both images the {010} form is prevalent.

EXPERIMENTAL METHODS

X-ray analysis and structure refinement

Among all the fragments available, only the smallest were not twinned and suitable for single-crystal X-ray diffraction study. Data collection was performed on a Bruker-AXS Smart-Apex CCD-based diffractometer with graphite-monochromatized Mo$K\alpha$ X-radiation. Crystal data are reported in Table 1.

Atom coordinates for the sites with highest electron densities were obtained by interpreting the Patterson synthesis in the Laue group *P2/m*. The position of the other atom sites was obtained by successive ΔF syntheses. The crystal structure was refined in the space group *P2/a* (no. 13), and the names of the cation sites were referred, as much as possible, to those of hellandite. Both structures have a unique octahedral site (M1) that is fixed at the origin, whereas the four independent tetrahedral sites of hellandite (Si1, Si2, B1, B2) double in piergorite-(Ce) (Si1A, Si1B, Si2A, Si2B, B1A, B1B, B2A, B2B). Furthermore, two eightfold coordinated M sites of hellandite (M3 and M4) increase to four in piergorite-(Ce) (M3A, M3B, M4A, M4B) while the $^{[8]}$M2 and the T site are not doubled. The crystal structure was refined by full-matrix least-squares cycles on *F*, using the program Crystals (Watkin et al. 2001). For atom sites in which isomorphous substitutions occur, the site population was obtained by refining the occupancy of two or three scattering factors for fully ionized chemical species, with their sum constrained to be 1. Results from electron and ion microprobe analyses were used to fix soft chemical restrains for species with similar scattering curves. Structure-refinement results are shown in Table 2 (atom coordinates and U_{eq}) and Table 3[1] (U_{ij}); selected bond lengths and angles are given in Table 4. Observed and calculated structure factors are listed in Table 5[1].

[1] Deposit item AM-06-019, Tables 3, 5, and 6. Deposit items are available two ways: For a paper copy contact the Business Office of the Mineralogical Society of America (see inside front cover of recent issue) for price information. For an electronic copy visit the MSA web site at http://www.minsocam.org, go to the American Mineralogist Contents, find the table of contents for the specific volume/issue wanted, and then click on the deposit link there.

TABLE 1. Crystal data for piergorite-(Ce)

a (Å)	28.097(3)
b (Å)	4.777(1)
c (Å)	10.236(2)
β (°)	96.81(1)
V (Å^3)	1364.2(7)
Space group	*P2/a*
Z	2
Size (mm)	0.01 × 0.07 × 0.11
D_{calc} (g/cm^3)	3.67
μ (cm^{-1})	63.32
Detector type	Smart-Apex CCD plate
Scan type	ω scans
Scan width (°)	0.1
Scan time (s)	60
Abs. correction*	Empirical
Total ref.	20419
2θ range (°)	2–70
Ref. with Io > 10σ(Io)†	3391
h range	–50 → 47
k range	–8 → 8
l range	–18 → 18
R_{int}	0.039
Unique ref.	8376
Obs. ref. $\|F_o\|>3\sigma(F_o)$	6480
R_{obs}	0.059
R_{all}	0.080
R_w	0.060
GoF	1.03

* SADABS software (Sheldrick 1996).
† Ref. used for unit-cell least-square refinement.

TABLE 2. Atom fractional coordinates, site multiplicity, site occupancy, refined site-scattering (ss, electrons), and equivalent isotropic atom-displacement parameters (U_{eq}·10⁴, Å²) in piergorite-(Ce)

Site	Mult.	Occupancy	ss	*x/a*	*x/b*	*x/c*	U_{eq}
B1A	4	1 B		0.2055(2)	0.4633(8)	–0.2688(4)	127(8)
B1B	4	1 B		0.1090(1)	0.4683(7)	–0.3024(3)	75(6)
B2A	4	1 B		0.1594(1)	–0.4597(6)	0.3516(3)	41(5)
B2B	4	1 B		0.1610(1)	–0.4667(6)	0.0887(3)	46(5)
Si1A	4	1 Si		0.0720(1)	–0.4999(2)	–0.0636(1)	65(2)
Si1B	2	1 Si		¼	–0.4967(3)	½	60(3)
Si2A	2	1 Si		¼	0.4846(3)	0	67(3)
Si2B	4	1 Si		0.0668(1)	–0.4797(2)	0.4400(1)	57(2)
M1	2	0.35(3) Fe + 0.49(2) Al + 0.16(5)Ti	18.99(4)	0	0	0	72(2)
M2	4	0.46(2) Ce + 0.39(1) Ca + 0.15(1)Th	47.98(11)	0.0271(1)	–0.0207(1)	–0.3248(2)	59(5)
M3A	4	0.98(3) Ca + 0.02 Ce	20.76(3)	0.1601(1)	–0.0088(2)	–0.1185(1)	80(2)
M3B	4	0.99(2) Ca + 0.01 Ce	20.38(4)	0.1580(1)	–0.0067(1)	–0.4445(1)	85(3)
M4A	4	0.99(3) Ca + 0.01 Ce	20.38(4)	0.1009(1)	0.0342(2)	0.2068(1)	89(3)
M4B	4	0.95(3) Ca + 0.05 Ce	21.90(3)	0.2188(1)	0.0092(2)	0.2401(1)	71(3)
T	4	0.27(7) Be + 0.15 Li	1.53(8)	0.0242(4)	0.4590(20)	0.1671(10)	46(10)
O1	4	1 O		0.2052(1)	–0.3206(5)	0.0369(2)	67(5)
O2	4	1 O		0.2307(1)	0.3055(6)	–0.1330(3)	148(7)
O3	4	1 O		0.2041(1)	–0.3107(5)	0.4348(2)	79(5)
O4	4	1 O		0.2310(1)	0.3149(5)	–0.3803(2)	88(5)
O5	4	1 O		0.0289(1)	–0.2418(5)	0.4686(2)	93(5)
O6	4	1 O		0.0832(1)	0.3313(5)	–0.4256(2)	80(5)
O7	4	1 O		0.1159(1)	–0.3214(5)	0.4018(2)	69(4)
O8	4	1 O		0.0464(1)	0.3115(6)	0.3220(3)	144(6)
O9	4	1 O		0.0329(1)	–0.2605(7)	–0.1112(3)	181(7)
O10	4	1 O		0.0846(1)	0.3239(5)	–0.1923(2)	104(6)
O11	4	1 O		0.0537(1)	0.2708(7)	0.0361(3)	172(7)
O12	4	1 O		0.1188(1)	–0.3308(5)	0.0040(2)	80(6)
O13	4	1 O		0.1614(1)	0.2406(5)	0.0812(2)	66(5)
O14	4	1 O		0.1601(1)	0.2481(5)	0.3618(2)	62(5)
O15	4	1 O		0.1066(2)	–0.2380(5)	–0.2998(2)	75(5)
O16	4	1 O		0.1594(2)	–0.3405(5)	0.2195(2)	63(5)
O17	4	1 O		0.2099(1)	–0.2457(5)	–0.2658(2)	72(4)
O18	4	1 O		0.1575(1)	0.3437(5)	–0.2852(2)	68(4)
O19	4	0.88(5) O + 0.12 F	8.12(8)	0.0241(2)	–0.1944(5)	0.1615(2)	95(5)

An amount of material for powder diffraction study was unavailable. Complete X-ray powder diffraction data (Table 6[1]) was simulated (for Cu$K\alpha$ X-radiation) combining the integrated intensities from single-crystal diffraction study at the proper 2θ values, taking multiplicities and Lp factors into account (XPREP software, Bruker-AXS Inc.).

Chemical data

The complete chemical analysis was obtained by means of electron microprobe analysis (EMPA) and secondary ion mass spectrometry (SIMS). WDS-EMPA was used to measure the intermediate-Z elements and was performed with a JEOL JXA-8600 electron microprobe at CNR-IGG (Florence). Analytical conditions were: 15 kV operating voltage, 80 nA beam current, a beam diameter of 5 μm. EMPA data relative to eight point analyses suggested a chemical homogeneity for the sample. The microprobe standards used were diopside (Ca), kaersutite (Si, Fe, Al, Mg), ilmenite (Ti), albite (Na), bustamite (Mn), and tugtupite (Cl). Data reduction was done using the PAP φ(ρZ) routine (Pouchou and Pichoir 1991).

An ion microprobe Cameca IMS 4f installed at CNR-IGG (Pavia) was used to quantify trace and minor elements spanning from low-Z (H, Li, Be, B) up to high-Z elements (REE, Th, U). The analytical procedures adopted were similar to those described in Ottolini and Oberti (2000). Moreover, additional elements were investigated in the present study, i.e., Sc, V, Cr, Rb, Zr, Nb, Cs, and Hf. Secondary-ion intensities were thus detected at the following masses (in amu): 30 (Si), 44 (Ca), 45 (Sc), 51 (V), 52 (Cr), 85 (Rb), 88 (Sr), 89 (Y), 90 (Zr), 93 (Nb), 133 (Cs), 137 (Ba), 139 (La), 140 (Ce), 141 (Pr), 146 (Nd), 149 (Sm), 163 (Dy), 167 (Er), 174 (Yb), 178 (Hf), 232 (Th), and 238 (U). Signals of Eu and Gd ion were obtained by deconvolution of the secondary-ion mass spectrum at mass numbers 151, 154, 160, and 162. The analysis of 1 (H), 7 (Li), 9 (Be), 11 (B), and 19 (F) was done on a different day to allow the crystal to degas at a vacuum of ~10^{-7} Pa with the proper H-reference samples in the dual specimen-holder inlet-chamber. $^{30}Si^+$ was used as the internal reference for the matrix for Li, Be, and B, and both $^{44}Ca^+$ and $^{30}Si^+$ were used as internal standards for the quantification of H and F. Analysis was done after 10 m bombardment at the same sites previously investigated for REE and other trace elements. To avoid any topographic effect due to the pre-existing craters, the crystal was polished smooth before analysis and then gold coated. We used apatite Snarum, britholite Los, NIST SRM 610 and LL St b as calibration standards (see Ottolini and Oberti 2000; Oberti et al. 2001). Moreover, hellandite D22 (Oberti et al. 2002) and medium-silica silicate standards (at disposal at SIMS lab, Pavia) were adopted as inner reference materials for the various trace elements selected. The SIMS data (average of two measurements) shows that Cr (2 ppm), Rb (1 ppm), and Cs (0.1 ppm) contents are comparable to our SIMS detection limits for such elements in silicates; Sc and Nb are present at about 20 ppm, whereas higher concentrations are reported for Hf (55 ppm), V (130 ppm), Ba (372 ppm), and Zr (1041 ppm). Quantification of Li, Be, and B was done following Ottolini et al. (1993). For Li, in addition, empirical corrections were carried out for the relative-to-Si ion yield for Li, IY(Li/Si), to take into account the different silica contents of our glassy standards relative to that of the sample. The overall accuracy was estimated as 5–10% for all the above elements. The analysis of F by SIMS was extremely demanding owing to the lack of a matrix-matched standard. Fluorine is a difficult element to investigate by EMPA and SIMS due to several kinds of matrix effects and artefacts (see Ottolini and Oberti 2000, and reference therein, for a general discussion). Britholite Los and other low-silica reference materials were used as calibration standards for H and F and the estimated accuracy is ~10% rel.

The resulting chemical composition of piergorite-(Ce) is given in Table 7 with the unit formula calculated on the basis of 38 (O, OH, F, Cl).

Crystal chemical features

The crystal structure of piergorite-(Ce) (Fig. 3) shows many analogies with that of hellandite. Briefly, the hellandite structure (Mellini and Merlino 1977; Oberti et al. 1999) consists of silicoborate chains $(Si_4B_4O_{22})^{-16}$ parallel to **c** in which two Si and three B tetrahedra define a five-membered ring (Fig. 4). A slightly distorted octahedron (M1) shares four vertices with different Si tetrahedra and interconnects adjacent tetrahedral chains. This structural arrangement defines tunnels along **c** filled by three cation sites (M2, M3, M4) in square antiprism coordination. The structure shows a very distorted tetrahedral cavity (T) between

TABLE 4. Selected bond distances (Å) and angles (°) in piergorite-(Ce)

B1A–O2	1.664(6)	M1–O9 ×2	1.987(3)	M4B–O1	2.601(2)	O9–Si1A–O10	108.9(1)
–O4	1.585(4)	–O11 ×2	1.989(3)	–O2	2.364(3)	O9–Si1A–O11	114.3(2)
–O17	1.396(4)	–O19 ×2	1.946(2)	–O3	2.583(2)	O9–Si1A–O12	105.2(2)
–O18	1.456(4)	Mean	1.974	–O4	2.388(2)	O10–Si1A–O11	105.9(2)
Mean	1.525			–O13	2.418(2)	O10–Si1A–O12	110.9(2)
		M2–O5	2.370(2)	–O14	2.462(2)	O11–Si1A–O12	111.6(2)
B1B–O6	1.526(4)	–O5′	2.380(2)	–O16	2.353(2)		
–O10	1.549(4)	–O6	2.600(2)	–O17	2.332(2)	O3–Si1B–O3	114.4(2)
–O15	1.405(4)	–O8	2.492(3)	Mean	2.438	O3–Si1B–O4 ×2	106.7(2)
–O18	1.478(4)	–O9	2.457(3)			O3–Si1B–O4 ×2	107.4(2)
Mean	1.490	–O10	2.577(3)	T–O8	1.779(11)	O4–Si1B–O4	114.3(2)
		–O15	2.449(2)	–O9	1.893(11)		
B2A–O3	1.599(4)	–O19	2.548(2)	–O11	1.886(11)	O1–Si2A–O1	111.1(2)
–O7	1.531(4)	Mean	2.484	–O19	1.657(11)	O1–Si2A–O2 ×2	107.4(2)
–O14	1.400(4)			Mean	1.804	O1–Si2A–O2 ×2	106.9(2)
–O16	1.467(4)	M3A–O1	2.424(2)			O2–Si2A–O2	117.3(2)
Mean	1.499	–O2	2.506(3)	O2–B1A–O4	102.4(3)		
		–O10	2.686(3)	O2–B1A–O17	113.9(3)	O5–Si2B–O6	110.9(2)
B2B–O1	1.571(4)	–O12	2.373(2)	O2–B1A–O18	102.4(3)	O5–Si2B–O7	107.9(2)
–O12	1.528(4)	–O13	2.363(2)	O4–B1A–O17	114.5(3)	O5–Si2B–O8	112.8(2)
–O13	1.401(4)	–O15	2.498(2)	O4–B1A–O18	103.5(3)	O6–Si2B–O7	106.6(2)
–O16	1.474(4)	–O17	2.452(2)	O17–B1A–O18	118.2(3)	O6–Si2B–O8	108.8(2)
Mean	1.493	–O18	2.392(2)			O7–Si2B–O8	109.6(2)
		Mean	2.462	O6–B1B–O10	101.7(2)		
Si1A–O9	1.620(3)			O6–B1B–O15	115.1(3)	O8–T–O9	105.4(5)
–O10	1.637(2)	M3B–O3	2.386(2)	O6–B1B–O18	105.4(2)	O8–T–O11	107.9(5)
–O11	1.622(3)	–O4	2.584(2)	O10–B1B–O15	113.9(3)	O8–T–O19	115.2(6)
–O12	1.626(2)	–O6	2.675(2)	O10–B1B–O18	102.4(2)	O9–T–O11	88.5(5)
Mean	1.626	–O7	2.386(2)	O15–B1B–O18	116.4(3)	O9–T–O19	119.5(6)
		–O14	2.333(2)			O11–T–O19	116.8(6)
Si1B–O3 ×2	1.641(2)	–O15	2.451(2)	O3–B2A–O7	103.7(2)		
–O4 ×2	1.659(2)	–O17	2.479(2)	O3–B2A–O14	113.6(2)	O9–M1–O11 ×2	96.9(2)
Mean	1.650	–O18	2.338(2)	O3–B2A–O16	103.4(2)	O9–M1–O19 ×2	92.8(2)
		Mean	2.454	O7–B2A–O14	114.2(2)	O11–M1–O19 ×2	91.6(2)
Si2A–O1 ×2	1.645(2)			O7–B2A–O16	103.2(2)	O9–M1–O11 ×2	83.1(2)
–O2 ×2	1.645(2)	M4A–O7	2.617(2)	O14–B2A–O16	117.0(2)	O9–M1–O19 ×2	87.2(2)
Mean	1.645	–O8	2.433(3)			O11–M1–O19 ×2	88.4(2)
		–O11	2.354(3)	O1–B2B–O12	102.2(2)		
		–O12	2.802(3)	O1–B2B–O13	114.4(2)		
Si2B–O5	1.608(2)	–O13	2.456(2)	O1–B2B–O16	103.6(2)		
–O6	1.664(2)	–O14	2.388(2)	O12–B2B–O13	113.8(2)		
–O7	1.660(2)	–O16	2.423(2)	O12–B2B–O16	103.7(2)		
–O8	1.618(3)	–O19	2.414(2)	O13–B2B–O16	117.4(2)		
Mean	1.638	Mean	2.486				

the silicoborate chains: the T site is occupied alternatively by Be and Li or vacant. The vacancy must be present when OH groups occur, because the H atom intrudes the T site, i.e., H apfu ≤ (2 – Be – Li – F) (Oberti et al. 1999).

Piergorite-(Ce) exhibits a more complicated tetrahedral motif than hellandite because B and Si tetrahedra are linked by corners to form a double chain of five-membered rings. Two Si sites (Si1B and Si2A), at the special position (1/4, *y*, 0), are shared between these two chains, resulting in the structural motif $(Si_6B_8O_{36})^{-24}$. The double chains are in the (010) plane and extend along **c**, this explains the similarity of the *b* and *c* cell parameters between piergorite-(Ce) and hellandite-type minerals (4.78 vs. 4.69–4.75 Å and 10.24 vs. 10.25–10.36 Å). Only the *a* cell parameter and the β angle change as a function of the different structural motifs (28.10 vs. 18.82–19.14 Å and 96.8 vs. 111.2–111.6°).

As in hellandite-type structures, the interconnection among silicoborate chains is guaranteed by a single $^{[6]}$M1 site, while a distorted tetrahedral cavity (T) connects two adjacent double chains at the same level of **b**. The doubling of the silicoborate chains in piergorite-(Ce) increases the space available for the eightfold coordinated sites, and five independent $^{[8]}$M sites (M2, M3A, M3B, M4A, and M4B) are present in the structure.

The silicoborate framework

X-ray single-crystal refinement shows that the isolated SiO_4 tetrahedra have <Si-O> bond lengths varying from 1.626 to 1.650 Å and are consistent with fully occupied Si sites. Si1A and Si2B share only two vertices with B tetrahedra and the distances with respect to the bridging (br) O atoms are longer than those of the non-bridging (nbr) O atoms. This is particularly evident for Si2B, for which the maximum differences between Si-O(br) and Si-O(nbr) distances is 0.056 Å. The other two Si sites share all vertices with different B tetrahedra resulting in more similar Si-O bond distances.

The B tetrahedra are arranged in two symmetrically independent B_2O_7 groups, characterized by five almost coplanar O atoms and two apical O atoms pointing in the same direction. Four of the basal O atoms connect the B_2O_7 groups to four different Si tetrahedra. Every B tetrahedron has bond distances with the apical oxygen always shorter than the other three (Δ_{max}= 0.268 Å for B1A), which suggests a displacement of the B atom from the center of the ideal tetrahedron toward the apical O(nbr). The displacement is also confirmed by the O-B-O bond angles, with the O(br)-B-O(br) angles significantly smaller (varying from 101.7 to 105.4°) and O(br)-B-O(nbr) angles significantly greater (from 113.6 to 117.4°) than the ideal value. The observed <B-O>

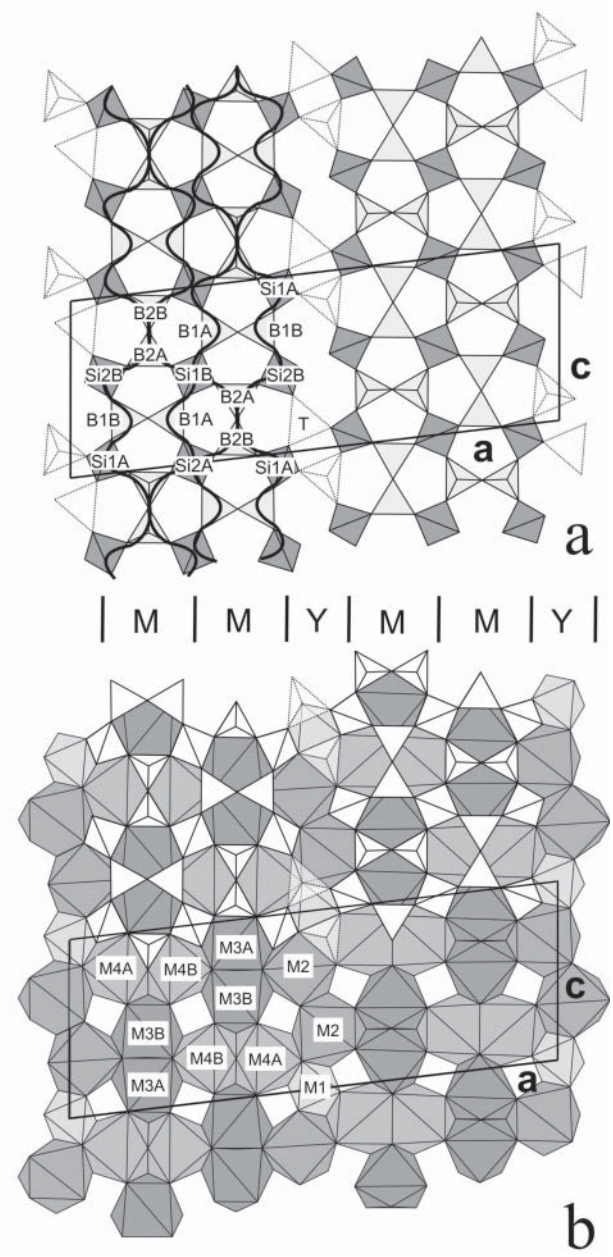

FIGURE 3. Projection along [010] of the crystal structure of piergorite-(Ce): (**a**) double chains of five-membered borosilicate rings and the partly populated T sites, represented with dashed lines (curves are a guide for the eyes to better show the two hellandite-like chains); (**b**) M sheet together with part of the overlapped tetrahedral layer. The sequence of M and Y structural blocks is also shown.

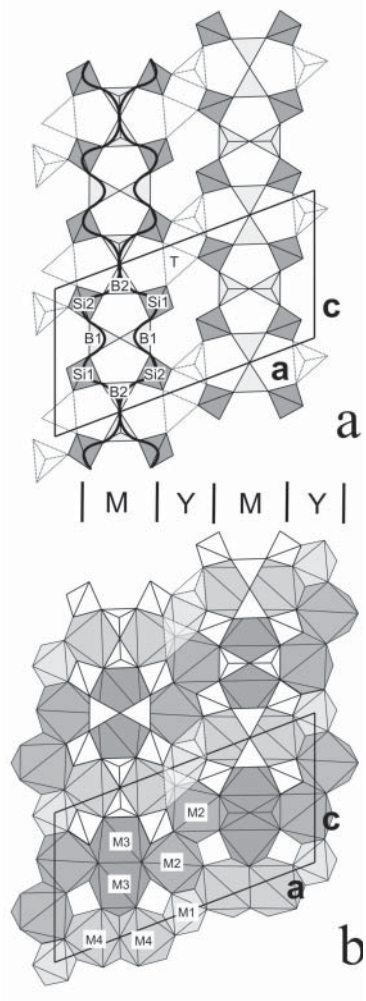

FIGURE 4. The same sketch of Figure 3 for hellandite-type structure.

distances are normal for B tetrahedra (Hawthorne et al. 1996); only <B1A-O> is a slightly longer (1.525 Å) primarily due to the particularly long value of B1A-O2 (1.664 Å). However, single tetrahedral distances longer than 1.67 Å are reported for borate minerals such as ruitenbergite (Grice et al. 1994) or cubic boracite (Sueno et al. 1973). The increased <B1A-O> value is probably due to local geometrical strains, because B1A is the only B-tetrahedron belonging to three different five-membered (Si, B) rings. Similarly, Si1B and Si2A tetrahedra are common among three five-membered rings and show longer <Si-O> values.

The extra framework site T and its relations with O19 population

The tetrahedral T site refines to a mean atomic number of 3.06 epfu, which is in very good agreement with the Be + Li content estimated by SIMS (corresponding to 2.91 epfu). Thus, all the Be and Li are located at this site. Also the refined <T-O> distance (1.804 Å) indicates the presence of a cation larger than Be [the mean bond distance for Be reported by Hawthorne and Huminicki (2002) is 1.633 Å]. The T tetrahedron involves the O19 site, the only one that is not connected with B or Si tetrahedra. The structure refinement results, together with the bond valence analysis (Table 8), suggest that F and OH species of the unit formula are located at this site. Diffraction data were unable to define the position of the H atom, however the atom arrangement around the O19 site in piergorite-(Ce) is the same as the corresponding anion site in the hellandite-type structure (O5). Therefore, in piergorite-(Ce) the H atom should intrude

the T position producing an overly short H-T distance, i.e., OH species must be absent when a T-cation occurs ($^{O19}OH \leq {}^{T}\square$). The O19 population is 0.35 O^{2-} + 0.76 F + 0.04 Cl + 0.85 OH apfu, and the OH content is less than the $^{T}\square$ (1.15 apfu).

The M polyhedra

The M1 octahedron shares four corners (two O9 and two O11) with four Si1A, allowing interconnections among tetrahedral chains along **a** and **b** axes: M1-O9 and M1-O11 distances (1.987 and 1.989 Å, respectively) are longer than M1-O19 (1.946 Å) for the OH and F content at this site. The refined site scattering (18.99 electrons) and the mean bond length (1.974 Å) suggest that M1 is primarily populated with Al and Fe^{3+}. Chemical analysis reports also a small Ti content together with minor Mn and Mg; all these chemical elements are hosted by the M1 site.

The eightfold coordinated M2 site shows the highest electron density (47.98 electrons) and is mainly populated by REEs and actinides; actually the bond valence analysis shows a higher charge for this site (Table 8). Like the M1 octahedron, the M2 polyhedron connects adjacent silicoborate chains both along **a** and **b** axes. The other eightfold coordinated polyhedra (M3A, M3B, M4A, and M4B) show similar electron densities (in the range 20.38–21.90 electrons) and are mainly populated by Ca. However, the <M-O> values are rather variable: M3A, M3B, and M4B have shorter mean distances (in the range 2.438–2.462 Å), whereas M4A has the same mean distance as M2 (2.486 Å) but M2 has very different cation populations (REE + actinides + Ca).

Discussion and comparison

The structure refinement of piergorite-(Ce) allows us to define the simplified crystal-chemical formula of this new mineral: $^{[M3A,M3B,M4A,M4B]}Ca_8{}^{[M2]}Ce_2{}^{[M1]}(Al_{0.5}Fe^{3+}_{0.5})_{\Sigma 1}{}^{[T]}(\square,Li,Be)_2Si_6B_8O_{36}(OH,F)_2$. Table 7 reports the complete unit formula on the basis of 38 (O, OH, F, Cl): the calculated tetrahedral population (6.02 Si

Table 7. Chemical analysis of piergorite-(Ce), unit formula calculated on the basis of 38 (O, OH, F, Cl), calculated (ssc) and observed (sso) site-scattering at M sites

	wt%		apfu
SiO_2	23.90	Si	6.02
B_2O_3	18.41	B	8.00
BeO	0.60		
Li_2O	0.48	Be	0.36
Fe_2O_3	2.09	Li	0.49
MnO	0.35	ΣT	0.85
TiO_2	0.71		
Al_2O_3	1.47	Fe^{3+}	0.40
MgO	0.06	Mn	0.07
CaO	31.06	Ti	0.13
Na_2O	0.01	Al	0.44
BaO	0.04	Mg	0.02
ThO_2	5.73	$\Sigma\,^{[6]}M$	1.06
UO_2	0.79		
ZrO_2	0.14	Ca	8.38
V_2O_5	0.02	Na	<0.01
Y_2O_3	0.44	Ba	<0.01
La_2O_3	3.33	Th	0.33
Ce_2O_3	6.24	U	0.04
Pr_2O_3	0.62	Zr	0.02
Nd_2O_3	1.57	V	<0.01
Sm_2O_3	0.15	Y	0.06
Eu_2O_3	0.02	La	0.31
Gd_2O_3	0.10	Ce	0.58
Dy_2O_3	0.07	Pr	0.06
Er_2O_3	0.04	Nd	0.14
Yb_2O_3	0.04	Sm	0.01
H_2O	0.50	Eu	<<0.01
F	0.96	Gd	0.01
Cl	0.10	Dy	<0.01
–O = F+Cl	0.43	Er	<<0.01
		Yb	<<0.01
Total	99.61	$\Sigma\,^{[8]}M$	9.96
	epfu	OH	0.85
$^{[6]}$Mssc	21.05	F	0.76
$^{[6]}$Msso	18.99	Cl	0.04
$^{[8]}$Mssc	269.48	O^{-2}	0.35
$^{[8]}$Msso	262.80	Σ O19	2.00

Table 8. Bond valence analysis (v.u.) of piergorite-(Ce)

Site	B1A	B1B	B2A	B2B	Si1A	Si1B	Si2A	Si2B	M1	M2	M3A	M3B	M4A	M4B	T	Total
Atom type	B	B	B	B	Si	Si	Si	Si	$Al_{0.49}Fe_{0.35}Ti_{0.16}$	$Ce_{0.46}Ca_{0.39}Th_{0.15}$	$Ca_{0.98}Ce_{0.02}$	$Ca_{0.99}Ce_{0.01}$	$Ca_{0.99}Ce_{0.01}$	$Ca_{0.95}Ce_{0.05}$	$Be_{0.27}Li_{0.15}$	
Site charge	3.00	3.00	3.00	3.00	4.00	4.00	4.00	4.00	3.16	2.76	2.05	2.01	2.01	2.05	0.69	
O1				0.58			x2↓ 0.95				0.29			0.19		2.01
O2	0.45						x2↓ 0.95				0.24			0.35		1.99
O3			0.54			x2↓ 0.96						0.32		0.20		2.02
O4	0.56					x2↓ 0.91						0.19		0.33		1.99
O5								1.05		0.47						1.98
O5′										0.46						
O6		0.66						0.9		0.25		0.15				1.96
O7			0.65					0.91				0.32	0.17			2.05
O8								1.02		0.34			0.29		0.17	1.82
O9					1.01				x2↓ 0.48	0.37					0.12	1.98
O10		0.62			0.97					0.27	0.15					2.01
O11					1.01				x2↓ 0.48				0.36		0.13	1.98
O12				0.66	0.99						0.34		0.11			2.10
O13				0.92							0.35		0.27	0.31		1.85
O14			0.93									0.38	0.32	0.27		1.90
O15		0.91								0.38	0.24	0.27				1.80
O16			0.77	0.76									0.29	0.36		2.18
O17	0.95										0.27	0.25		0.39		1.86
O18	0.79	0.75									0.32	0.37				2.23
O19									x2↓ 0.54	0.29			0.3		0.23	1.36
Total	2.75	2.94	2.89	2.92	3.98	3.74	3.80	3.88	3.00	2.83	2.20	2.25	2.11	2.40	0.65	

Note: The valence of each site take account of the contribution of different atom species; bond valence calculated after Brown and Altermatt (1985) with the parameters given by Brese and O'Keeffe (1991).

+ 8.00 B apfu) from the microchemical data matches exactly the tetrahedral sites (6 + 8) of the silicoborate chains. The number of largest cations in the unit formula (9.96 apfu) agrees with the number of largest [8]M cavities (10) and also the Al + Fe^{3+} + Ti^{4+} + Mn^{+2} + Mg (1.06 atoms) is compatible with the unique octahedral cavity (M1). The electron density of the M cations (290.53 epfu) is in excellent agreement with the refined site-scattering at the [8],[6]M sites (281.79 epfu), the discrepancy of ~3% is within the analytical uncertainty of the adopted analytical techniques.

The structural motif of piergorite-(Ce) ($Si_6B_8O_{36}$) can be derived from that of hellandite ($Si_4B_4O_{22}$) by means of a doubling of the silicoborate chains that extend along **c**. In hellandite, the single silicoborate chains are always constituted by the same five-membered ring (2B1 + B2 + Si1 + Si2 tetrahedra) linked by corners; in piergorite-(Ce), two hellandite-like chains are connected by sharing of the Si1B and Si2A tetrahedra. The resulting double chain is formed by 3 different five-membered rings: (1) B1A + B1B + B2A + Si1B + Si2B; (2) B1A + B1B + B2B + Si1A + Si2A; (3) B1A + B2A + B2B + Si1B + Si2A. The different structural motifs involve a different SiO_2/B_2O_3 ratio in the chemical analysis of the two phases: 1.3 in piergorite-(Ce) and ~1.7 in hellandites.

Both piergorite-(Ce) and hellandite become sheet minerals when the T site is entirely occupied. When this is the case, two additional rings of tetrahedra occur: an eight-membered ring formed by 2Si1A + 2B1B + 2Si2B + 2T in piergorite-(Ce) (2Si1 + 2B1 + 2Si2 + 2T in hellandite) and a four-membered ring formed by 2Si1A + 2T in piergorite-(Ce) (2Si2 + 2T in hellandite).

The tetrahedral layers alternate along **b** with a sheet composed of M sites. In piergorite-(Ce), the [6]M1 and two [8]M2 (related by the inversion center) form chains of edge sharing polyhedra that extend along **c** with the same arrangement of hellandite-like structures. The other [8]M sites (M3A, M3B, M4A, M4B) form along **c** two symmetrically equivalent chains of edge-sharing polyhedra, each one very similar to the single M3-M4 chain of hellandite.

The structural relationships between piergorite-(Ce) and hellandite minerals can be explained by using a sequence of bidimensional blocks, defined by subsequent slicing planes parallel to (100) and passing through the Si sites (Figs. 3 and 4). Two kinds of blocks are present: the M block containing the B_2O_7 groups; the Y block containing the T tetrahedra (Be, Li, vacant). The resulting sequences are MMYMMY… for piergorite-(Ce) and MYMY… for hellandite minerals. Interestingly, the absence of the Y block defines the MMMM… sequence that characterizes the topology of meliphanite (Grice and Hawthorne 2002). Namely, piergorite-(Ce) and hellandite minerals are various members of a polysomatic series built by modules M (related to meliphanite) and Y. If other members of this series are found (e.g., MMMYMMMY…, etc.), their *b* and *c* cell parameters should be similar to those of piergorite-(Ce) and hellandite.

Notwithstanding the different number of independent [8]M cavities, piergorite-(Ce) and hellandite minerals show the same distribution of the chemical elements in these sites. In particular, elements with higher atomic number and formal charge (REEs and actinides) are preferentially located in the same M site (M2). These analogies in the site population probably reflect the similar arrangement of the M polyhedra in both structures. In particular,

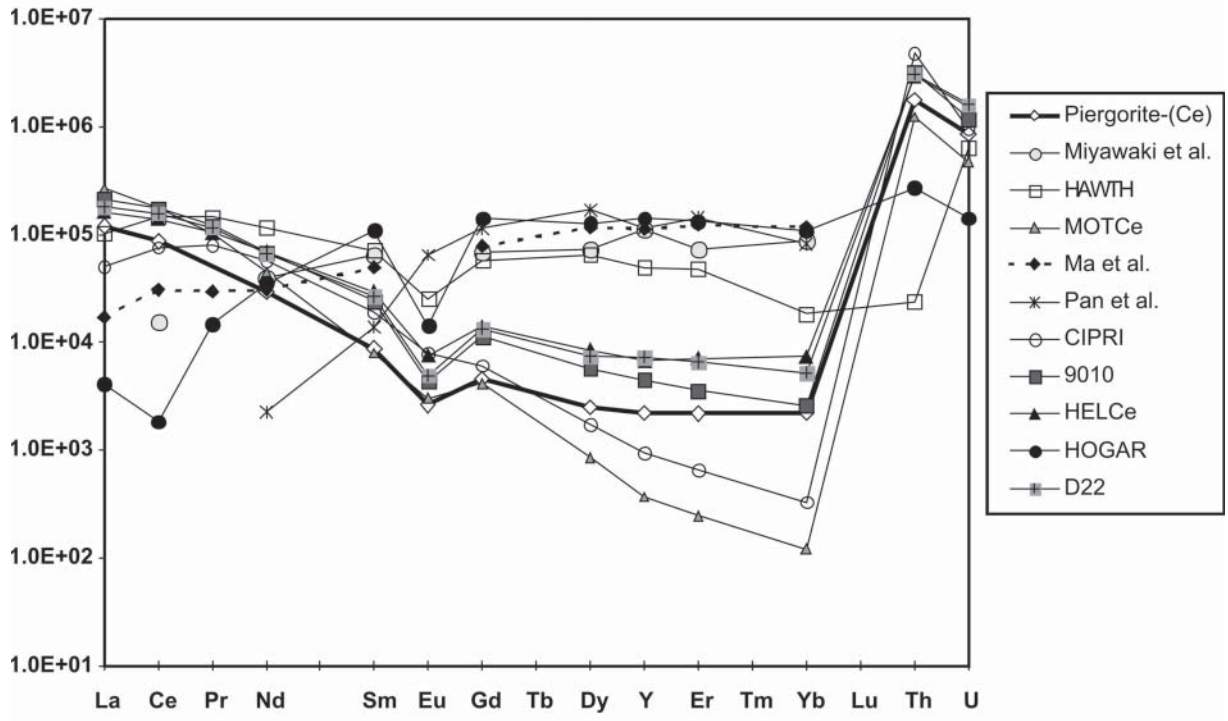

FIGURE 5. Chondrite-normalized REE pattern for piergorite-(Ce) and hellandites from several localities [piergorite-(Ce) pattern is drawn with a bolder line; see Oberti et al. (2002) for hellandite references].

the [6]M1 and [8]M2 chains, together with the borosilicate chains, define the structural channels that contain all the other [8]M sites and any change in their composition affects the dimension of the channels, in particular increasing the spacing along **b**.

The C1-chondrite-normalized REE pattern of piergorite-(Ce) is reported in Figure 5, together with the C/C1 patterns of several hellandites from different localities, for comparison. It shows an enrichment in the LREE region and a linear decrease toward MREE region, with a negative Eu anomaly (Eu/Eu* = 0.06). The pattern decreases slowly in the HREE region to increase again in Th and U. Previous studies show that REE-pattern of hellandites are very variable and mainly influenced by the environment of formation. The Eu anomaly is always present in all the samples studied (Oberti et al. 2002), and is presumably related to the presence of the coexisting K-feldspar (sanidine). The REE (Th, U)-pattern for piergorite-(Ce) is similar in shape (albeit with lower concentrations) to that of the hellandites of the same district, i.e., samples D22 and Hel-Ce (Oberti et al. 2002) both formed in a syenitic ejectum in Viterbo province (Vetralla and Capranica localities, respectively). However, a very complete list of constituents has been obtained for the first time for a phase that strongly resembles the hellandite-type matrix.

Classification and nomenclature

On the basis of the results of this work, piergorite-(Ce) (with the hellandite minerals) can be classified in Dana Class 54.2 of the borosilicates and some beryllosilicates, and in 9.DK.15 of the Strunz and Nickel (2001) classification. It can be also classified among the mixed silico-borate minerals with 2□ connectivity, following Hawthorne et al. (1996). However, piergorite-(Ce) must be considered as the first end-member of a new mineralogical group based on the presence of the new $Si_6B_8O_{36}$ structural motif. The crystal-chemical study of this new mineral shows that several substitutions (heterovalent or homovalent) occur: [6]M1 can host homovalent couples (Al and Fe^{3+}) and also tetravalent species (Ti^{4+}); [8]M2 is populated by Ca and REEs but can host Th^{4+} and other heterovalent cations (Zr, U, Ba, Na); O19 can be a monovalent (OH or F) or a bivalent anion (O^{2-}). Therefore, piergorite-(Ce) shows the same crystal chemical variations as hellandite minerals and a nomenclature scheme that follows the rules of hellandites (Oberti et al. 2002) can be proposed: different root names shall be adopted for piergorite-group end-members when R^{4+} cations fill the M1 (Ti^{4+}) or M2 (Th^{4+}) site, and further root names shall be used to identify composition with the tetrahedral T site filled (by Li or Be). A Levinson modifier shall be used to identify the dominant REE at the [8]M2 site. Because of the octahedral population in piergorite-(Ce) (~½ Al and ½ Fe^{3+}), it is plausible to hypothesize the use of an adjectival modifier for end-members in which a dominant trivalent species is present at the [6]M1 site.

Acknowledgments

Sincere thanks are due to Filippo Olmi from CNR-IGG, Florence for EMP analyses; his untimely passing is mourned by all of us. Thanks are also due to Olaf Medenbach from the Institute of Geology, Mineralogy and Geophysics Mineralogy, University of Bochum, for the precise measurements of refractive indices. The authors are grateful to the reviewers S. Merlino and J.D. Grice and to the Associate Editor, P. Bonazzi for their suggestions that greatly improved the manuscript. In particular, we are much indebted to S. Merlino, who suggested the description of this mineral as a member of a polysomatic series, and to J. D. Grice, who allowed us to correct an error in the approved mineral name.

The Italian CNR is acknowledged for financing the ion microprobe at the Istituto di Geoscienze e Georisorse (IGG)-CNR, Pavia.

References cited

Ballirano, P., Callegari, A., Caucia, F., Maras, A., Mazzi, F., and Ungaretti, L. (2002) The crystal structure of vicanite-(Ce) a borosilicate showing an unusual $(Si_3B_3O_{18})^{15-}$ polyanion. American Mineralogist, 87, 1139–1143.

Brese, N.E. and O'Keeffe, M. (1991) Bond-valence parameters for solids. Acta Crystallographica, B47, 192–197.

Brown, I.D. and Altermatt, D. (1985) Bond-valence parameters obtained from a systematic analysis of the inorganic crystal structure database. Acta Crystallographica, B41, 244–247.

Callegari, A., Giuseppetti, G., Mazzi, F., and Tadini, C. (1992) The refinement of the crystal structure of stillwellite: RE($BSiO_5$). Neues Jahrbuch für Mineralogie Monatshefte, H.2, 49–57.

Callegari, A., Caucia, F., Mazzi, F., Oberti, R., Ottolini, L., and Ungaretti, L. (2000) The crystal structure of peprossiite-(Ce), an anhydrous REE and Al mica-like borate with square-pyramidal coordination for Al. American Mineralogist, 85, 586–593.

Della Ventura, G., Parodi, G.D., and Stoppani, F.S. (1986) Minerali del Lazio (1). Rivista Mineralogica Italiana, 4, 157–166.

Grice, J.D. and Hawthorne, F.C. (2002) New data on meliphanite, $Ca_4(Na,Ca)_4Be_4AlSi_7O_{24}(F,O)_4$. Canadian Mineralogist, 40, 971–980.

Grice, J.D., Burns, P.C., and Hawthorne, F.C. (1994) Determination of the megastructures of the borate polymorphs pringleite and ruitenbergite. Canadian Mineralogist, 32, 1–14.

Hawthorne, F.C. and Huminicki, D.M.C. (2002) The crystal chemistry of beryllium. In E.S. Grew, Ed., Beryllium: Mineralogy, Petrology and Geochemistry, 50, p. 333–403. Reviews in Mineralogy and Geochemistry, Mineralogical Society of America, Chantilly, Virginia.

Hawthorne, F.C., Burns, P.C., and Grice, J.D. (1996) The crystal chemistry of boron. In E.S. Grew and L.M. Anovitz, Eds., Boron Mineralogy, Petrology and Geochemistry, 33, p. 41–115. Reviews in Mineralogy, Mineralogical Society of America, Chantilly, Virginia.

Mandarino, J.A. (1981) The Gladstone–Dale relationship, IV. The compatibility concept and its application. Canadian Mineralogist, 19, 441–450.

Mellini, M. and Merlino, S. (1977) Hellandite: a new type of silicoborate chain. American Mineralogist, 62, 89–99.

Oberti, R., Ottolini, L., Camara, F., and Della Ventura, G.C. (1999) Crystal structure of non-metamict hellandite-(Ce) from Latium (Italy) and crystal chemistry of the hellandite-group minerals. American Mineralogist, 84, 913–921.

Oberti, R., Ottolini, L., Della Ventura, G.C., and Parodi, G.C. (2001) On the symmetry and crystal chemistry of britholite: New structural and microanalytical data. American Mineralogist, 86, 1066–1075.

Oberti, R., Della Ventura, G.C., Ottolini, L., Hawthorne, F.C., and Bonazzi, P. (2002) Re-definition, nomenclature and crystal-chemistry of the hellandite group. American Mineralogist, 87, 745–752.

Ottolini, L. and Oberti, R. (2000) Accurate quantification of H, Li, Be, B, F, Ba, REE, Y, Th, and U in complex matrixes: A combined approach based on SIMS and single-crystal structure refinement. Analytical Chemistry, 72, 3731–3738.

Ottolini, L., Bottazzi, P., and Vannucci, R. (1993) Quantification of lithium, beryllium, and boron in silicates by secondary ion mass spectrometry using conventional energy filtering. Analytical Chemistry, 65, 1960–1968.

Pouchou, I. and Pichoir, F. (1991) Quantitative analysis of homogeneous or stratified microvolumes applying the model "PAP". In K.F.G. Heinrich and D.E. Newbury, Eds., Electron Microprobe Quantitation, p. 31–75. Plenum Press, New York.

Sheldrick, G. M. (1996) SADABS Siemens area detector absorption correction program. University of Göttingen, Germany.

Sueno, S., Clark, J.R., Papike, J.J., and Konnert, J.A. (1973) Crystal-structure refinement of cubic boracite. American Mineralogist, 58, 691–697.

Strunz, H. and Nickel, E.H. (2001) Strunz Mineralogical Tables. Chemical-structural mineral classification system (9th edition). Schweizerbart, Stuttgart, Germany.

Watkin, D.J., Prout, C.K., Carruthers, J.R., Betteridge, P.W., and Cooper, R.I. (2001) Crystals issue 11. Chemical Crystallography Laboratory, Oxford, U.K.

Manuscript received November 8, 2005
Manuscript accepted March 5, 2006
Manuscript handled by Paola Bonazzi